Deconstruction of tropospheric chemical reactivity using aircraft measurements: the ATom data

Hao Guo* and Michael J. Prather*

Department of Earth System Science, University of California, Irvine, CA 92697 USA

* *Correspondence to:* Hao Guo (haog2@uci.edu) and Michael J. Prather (mprather@uci.edu).

Abstract.

From NASA's Atmospheric Tomography (ATom) mission, we calculate the average production/loss of O_3 and CH_4 for 10s air parcels along profiling transects through the Pacific/Atlantic Oceans for four seasons. We find photochemically hot air masses on all scales from 2 to 2000 km. Tropical production of O_3 is high (~2 ppb/day) throughout the ATom profiles (0–12 km). In the Eastern Pacific we find large coherent air masses of extremely high reactivities in August (monsoonal) and May (biomass burning). The tropics dominate the O_3 and CH_4 budgets. Sensitivity analysis identifies only five critical species (NOx, O_3, CH_4, CO, and H_2O) responsible for driving the budgets. Sensitivity analysis shows large 2^{nd}-order effects for coupled perturbations, indicating that 1^{st}-order sensitivities cannot simply be added. Feedback analysis indicates a slower-than-expected timescale for decay of O_3 perturbations. ATom data shows how global tropospheric chemistry is constructed from a myriad of fine and large scales.

1. Introduction

The environmental damage caused by chemically reactive greenhouse gases and air pollutants is controlled by a balance between sources and sinks, with the major sink usually being atmospheric photochemistry. The net chemical loss is a key budget term, and it comprises a highly heterogeneous mixture of air parcels, each with its own mix of species, and each with its own chemical production and/or loss rates designated here as the reactivities: P-O3, L-O3, and L-CH4 (see Prather et al., 2017; 2018, hence P2017 and P2018). Reactivity here is simply the 24-hour integration of a reaction rate, or the sum of several reaction rates, that describe budgets of species in units of ppb per day. In this paper we continue our efforts to understand how tropospheric chemistry is constructed by examining reactivities starting at the finest spatial scales.

A recent observation-based study of the chemical reactivity of individual air parcels used the 10 s in situ aircraft measurements from the NASA Atmospheric Tomography (ATom) mission's first deployment (ATom-1; Guo et al., 2021, hence G2021). Recent publications have identified new scientific opportunities coming from ATom with its intensive, chemically comprehensive measure of composition combined with an extensive, semi-global profiling through the remote troposphere (Wofsy et al., 2018; Thompson et al., 2021). Topics include scales of variability (Schill et al., 2020; G2021), global CO forecasting (Strode et al., 2018), and OH oxidative capacity (Wolfe et al., 2019; Brune et al., 2020;

Travis et al., 2020; Anderson et al., 2021; G2021), as well as areas unrelated to this work, such as aerosol distribution, formation, and precursors (Brock et al., 2021; Williamson et al., 2021; Veres et al., 2020).

Here we extend G2021 to report reactivities for all four seasonal deployments (ATom-1234, see Figure S1) and examine how their statistical patterns change with each deployment. Second, we perform sensitivity analyses to identify which of the ATom-measured species drives the reactivities, and thus which are critical for the chemistry-climate models (CCMs) to simulate accurately. Third, probability densities for these critical species from ATom are presented as possible performance metrics for CCMs.

Our interests in the reactivity of air parcels or model grid cells began with P2017, continuing with P2018 and G2021. We focused on the budgets of O_3 and CH_4, and reactivities were defined by some key reaction rates:

loss of CH_4 (L-CH4),

CH_4 + OH CH_3 + H_2O (1)

production of O_3 (P-O3),

HO_2 + NO NO_2 + RO (2a)

RO_2 + NO NO_2 + RO (2b)

O_2 + h O + O (x 2) (2c)

and loss of O_3 (L-O3),

O_3 + OH O_2 + HO_2 (3a)

O_3 + HO_2 HO + O_2 + O_2 (3b)

$O(^1D)$ + H_2O OH + OH (3c)

These rates are readily calculated in most CCMs, and we found that the net P-O3 minus L-O3 accurately described the 24 h O_3 tendencies over the ocean basins but not in highly polluted boundary layers. Reaction 2c is important in the upper tropical troposphere (Prather, 2009), but only above ATom flight levels. The calculation of reactivities here use the UCI model and the RDS*-2 protocol described in G2021.

We mainly consider the Pacific and Atlantic oceanic flights of ATom, which we constrain to be 54°S to 60°N (see the included flights in Figure S2), but also include a focus on the tropical flights (30°S to 30°N), splitting the Pacific flights into Central and Eastern Pacific (0°-30°N only). Reactivities at latitudes poleward of 60° are smaller than over the oceans, and we present a less extensive analysis for the Arctic and Antarctic.

Latitude-by-altitude curtain plots of the reactivities along flight tracks are presented in Section 2, along with altitude profiles of the mean reactivities and probability densities over the ocean basins. In Section 3 we present our analysis

of the sensitivity of the reactivities to ATom MDS species, identifying those critical species where a model bias will introduce large errors in the O_3 and CH_4 budgets. Critical species probability densities from ATom are introduced in Section 4 as a possible model metric, and Section 5 concludes this analysis.

2. Variation of photochemical reactivities across the four ATom deployments

2.a. Curtain plots

The spatial structures and variability of P-O3 as sampled by the ATom transects over the Pacific Ocean are presented in Figure 1a. The full set of plots covering all three reactivities and also the Atlantic Ocean are shown in Supplementary Figures S3-S8. For these curtain plots, the 10 s reactivities (2 km by 80 m thick parcels) are averaged and plotted in 1° latitude by 200 m thick cells. In August (ATom-1), the highly reactive (hot) P-O3 parcels (3.5 to 6+ ppb/day) are common throughout most of the lower troposphere (0-5 km) from 20°S to 60°N, and there is also a region of very high P-O3 in the upper northern tropics (8-12 km, 15°N-30°N). In February (ATom-2), P-O3 shifts to the southern mid-latitude and tropics following the overhead sun as expected, but the tropical production lacks the intensity seen in ATom-1 in the 20°N-30°N region. In October (ATom-3) the high P-O3 parcels are primarily tropical, but favor the southern latitudes. Finishing in May (ATom-4) we find the northern dominance returns although not as strongly as in ATom-1 and find some regions of P-O3 > 5 ppb/day as also in ATom-1. Overall, this shows the dominance of the tropics for production of O_3 over the oceans. The northern summer mid-latitudes almost contribute a fifth tropical season, and all of the highly reactive regions probably show the importance of deep convection over northern continents influencing the tropical Pacific in August and May. The loss of O_3 shows similar seasonal shifts as P-O3, following the sun especially in the tropics, and moving into the northern mid-latitudes in August and May, but high reactivities are limited to below 8 km. The loss of CH_4 parallels that of O_3.

In the Atlantic P-O3 also follows the sun, with high reactivity south of the equator for February (ATom-2) and October (ATom-3). In August (ATom-1), a substantial number of air parcels show high P-O3 (2-6 ppb/day) from 10°S to 45°N. There is a cluster of hot parcels in the lower troposphere (1-5 km) but also a clustering in the upper troposphere (6-12 km), including about 20°S in May (ATom-4). We know that the tropical Atlantic O_3 is influenced by continental outflow of biomass burning from South America and Africa (Fishman et al., 1990), and here we see that outflow is actively producing O_3. L-O3 occurs in a more tightly constrained region than P-O3, both in latitude and altitude (0-6 km). L-O3 is centered on the tropics for all Atom-1234 but, like in the Pacific, it includes a highly reactive region in northern summer mid-latitudes (30°N-50°N, ATom-1). The Atlantic pattern of L-CH4 is almost identical to that of L-O3, but peaks about 1 km lower in altitude.

Given the importance of the tropics in the global reactivity of the atmosphere,

we create expanded 30°S-30°N curtain profiles and separate the Pacific into Central (about 180°E-210°E) and Eastern (about 240°E, the first flight of each deployment from Palmdale CA south to the equator and back) (Figures S9-S17). The expanded plots clearly show the patchy nature of P-O3 hot spots in the Central Pacific and the Atlantic (except for 15°S-25°S, 7-9 km), while emphasizing the large coherent hot spots in L-O3 and L-CH4 in the Atlantic. The Eastern Pacific stands out: there are large coherent regions (20° by 2-3 km) associated with well mixed convective outflow from North America having extreme reactivities in August (monsoonal) and May (possibly biomass burning).

Curtain profiles for the Arctic (Figure S18) are presented only for ATom-1 and ATom-4 when there was enough sunlight to generate non-negligible reactivities. The stratospheric air parcels are excluded. Reactivities appear moderately high, but the color scale here is 3 times smaller than in Figures S3-S17. In the Arctic, much of the P-O3 occurs above 6 km, and L-CH4 is suppressed relative to L-O3 because of the colder temperatures. Only one of the two Antarctic flights had enough sunlight to produce much reactivity (ATom-3, Figures S19). Like the Arctic, P-O3 is in the upper troposphere, while L-O3 and L-CH4 are in the lower. Note that the color scale is 6-to-12 times smaller than in Figures S3-17.

2.b. Mean altitude profiles

Altitude profiles of the mean P-O3 for the three tropical basins and the 4 deployments are compared in Figure 1b (for other regions and reactivities, see Figures S20-S27). For Central Pacific and Tropic Atlantic, the variation across deployments is not so large with values ~2 ppb/day throughout. ATom-1, however, shows slightly higher P-O3 (~3 ppb/day) below 4 km in both regions and also in the upper troposphere but only in the Atlantic.

In the Eastern Pacific, however, each deployment seems unique: ATom-2 is almost uniform at 2 ppb/day; ATom-134 show enhanced upper troposphere P-O3 probably from deep convection and lightning NOx over North America; ATom-13 show large mid-tropospheric production of ~3 ppb/day not seen in ATom-24; and ATom-4 finds a thick atmospheric layer, 1-3 km, with an astounding rate of P-O3, averaging ~10 ppb/day. The end of the biomass burning season in Central America (15°N-20°N) is probably the cause of the peak P-O3 in ATom-4 (May); while the start of the North American Monsoon season is probably the cause of the extensive deep-convection layer (8-12+ km) with high P-O3 in ATom-1 (August). With this high level of variability, it will be important to re-examine the time period of the ATom flights with a chemistry-transport model to assess the spatio-temporal scales of these incredible events. As expected from Figure 1a, the lowest P-O3 in all 3 tropical basins occurs in northern winter (ATom-2, February). For L-O3 and L-CH4, the Central Pacific and Tropical Atlantic show little variability across ATom-1234, but the Eastern Pacific shows the extremely high reactivities for ATom-14 as found in P-O3 (Figures S23-S25).

In the Arctic (Figure S26) ATom-14 show nearly identical and constant profiles for all 3 reactivities; while ATom-23 have negligible reactivities. P-O3 peaks at

8-12 km with values from 1-2 ppb/day. The reactivities in the Arctic, even in summer are less than the average over the Pacific and Atlantic oceans and thus have little impact on the global O_3 or CH_4 budgets. In the Antarctic (Figure S27), reactivities are much less than the Arctic and only reported for ATom-3.

2.c. Probability densities of photochemical reactivities

The probability densities (PDs) of the ATom reactivities have proven useful in testing model climatologies (see G2021). Here, we plot the PDs for the 4 deployments in the major oceanic regions for all 3 reactivities (Figures S28-S33). Overall, we find ATom-1 has more frequent high reactivities, and the East Pacific has the least conformity across ATom-1234. The Central Pacific and Tropical Atlantic provide a repeatable pattern that should provide an excellent test for CCM climatologies.

3. Sensitivity analysis

To identify the critical species controlling the tropospheric budgets of O_3 and CH_4, we calculate the sensitivity of the weighted mean reactivity for the Pacific or Atlantic oceanic flights of ATom (54°S to 60°N) with respect to the species measured by ATom. Sensitivity analyses are often calculated with CCMs, for example, to assess the factors controlling trends and variability in CH_4 lifetime (Holmes et al., 2013). In that case the species abundances as well as the chemistry module calculating the reactivities (e.g., L-CH4) are based on the emissions, transport and chemistry in the CCM. Here, we use the ATom observations to initialize the species needed for the chemistry module and then calculate the reactivities (see P2018). Our goal is also different: to recognize the errors in modeled budgets caused by errors in initial values of the species.

The sensitivity S of reactivity R to species X is calculated from the fractional change in R per fractional change in X (dimensionless, e.g., %/%). We use Δ = 10%.

$$S \quad \ln(R) / \ln(X) = \ln(R[X(1+\Delta)] / R[X]) / \ln(1+\Delta) \quad (4)$$

Results from 13 species for the 3 reactivities, the Pacific and Atlantic basins, and 4 ATom deployments are given in Table S1. The variability across basins and deployments is small, and we summarize the mean and standard deviation of the 8 S values in Table 1. Surprisingly, the initial value of many species (HCHO, H_2O_2, PAN, HNO_3, HNO_4, CH_3OOH, C_2H_6, C_{3+}-alkanes) has little impact on the reactivities, and these are not shown in Table 1. The only one of these species that breaks the $S > 0.10$ barrier is CH_3OOH for P-O3 in the Pacific.

The lessons from Table 1 are quite interesting: (i) as expected, NOx is important for P-O3 but not much more so than O_3, CH_4, and H_2O; (ii) NOx is the least important for L-CH4 of the 5 species in Table 1; (iii) H_2O is important across all reactivities; (iv) the sensitivity of L-CH4 to CH_4 (0.71) shows that the OH-driven loss of CH_4 decreases with a sensitivity of -0.29; and surprisingly, (v) the increase in net loss of O_3 (P-O3 minus L-O3) with increasing O_3 concentrations

is driven primarily by reduced P-O3 rather than increase L-O3. In detail, if O_3 increases by 10%, then L-O3 increases by 2.5% but P-O3 decreases by 5.4%, and thus net loss increases by 7.9% (i.e., net L-P sensitivity = 0.79). Our analysis presents quite a different picture for the decay of O_3 than is assumed in many modeling studies where the decay of stratospheric ozone entering the troposphere assumes the sensitivity of L-O3 with respect to O_3 is exactly 1.0 (Roelofs and Lelieveld, 1997; Abalos et al., 2020). The CH_4 feedback factor derived here from the sensitivities (-0.29) is well within the range calculated by global models (Holms et al., 2013; Holmes, 2018), but it is only a 24-hour feedback and does not include the impact of increasing CH_4 on CO and O_3 concentrations that would only appear in a few months. Our sensitivity of L-CH4 to NOx (0.09) is similar to Holmes et al. (2013), but theirs is larger (0.16) because they only considered lightning NOx, which generally has a larger impact on photochemistry than other sources of NOx. Their sensitivity to H_2O (0.32) is close to ours (0.38). So there is nothing new here, except for the O_3 sensitivities, but we have shown that these sensitivities can be derived from an observational data set.

We examined the second-order quadratic nature of our S values by re-calculating with $\Delta = 20\%$, but the results hardly changed (Table S2). Thus, quadratic terms are not important for perturbations <20%. The second-order cross-species terms are far more interesting. We calculate these from a coupled 10% perturbation of 2 different variables

$$S_{XY} = S(X{+}10\% \;\&\; Y{+}10\%) - S(X{+}10\%) - S(Y{+}10\%) \quad (5)$$

and define 2nd-order term S_{XY} as the additional change in sensitivity due to the combined perturbation. We examine S_{XY} using only 4 species (NOx, O_3, CH_4, CO) and highlight L-CH4 in the ATom-1 Pacific basin in Table 2, while the other reactivities and Atlantic basin (also only for ATom-1) are shown in Table S3. The diagonal elements in the 4x4 array of Table 2 are simply the 1st-order sensitivities, S(X+10%), shown also in Table S1. The off-diagonal elements in each array are S_{XY}, and these are doubly signed (i.e., ++ or --) for emphasis. If $S_{XY} \sim 0$, then the coupled perturbation is just the sum of the 1st-order terms.

Surprisingly, we find strong co-effects for combined perturbations that are similar in magnitude to the 1st-order sensitivities. For example, for L-CH4 in the Pacific (Table 2), the total sensitivity for NOx (+0.09) plus O_3 (+0.39) is reduced by 27%, 0.09+0.39–0.13 = +0.35. Likewise, the combined NOx plus CO sensitivity is also reduced in absolute magnitude by about 50%, 0.09–0.34+0.12 = –0.13. For P-O3, the S_{XY} are also large compared to the 1st-order sensitivities; but for L-O3, the only major 1st-order sensitivity among these 4 species is to O_3 itself, and the 2nd-order S_{XY} terms are much smaller (Table S3). L-O3 does have large 1st-order terms for H_2O (Table 1), but we did not calculate 2nd-order S_{XY} for these. In terms of net P–L for O_3, the S_{XY} terms partly cancel each other (i.e., enhancing both P and L) except for the NOx-CO pair: the combined NOx plus CO perturbation has a net P–L sensitivity of +0.16+0.06+0.11 = +0.33, 50% larger than the sum of 1st-order terms.

When modelers explore factors driving changes in the lifetime of CH_4 (e.g., Holmes et al., 2013), it is essential to recognize that coupled perturbations cannot be derived simply from the 1st-order sensitivities. We note that although this study used ATom MDS data to represent the remote troposphere, it could have been done anytime over the past several decades using the distribution of species in 3D global models. An interesting result here is that when we use the UCI CTM distribution of chemical species, we calculate similar sensitivities even though the modeled species distributions are different from the observed ATom distributions (see Fig. 4 of G2021). Possibly, the sensitivities depend more on the chemistry module than on the distribution of species. Thus, we urge a multi-model comparisons of tropospheric chemistry sensitivities to use the ATom data as the observational basis.

This result is not surprising if one recognizes that most reactions are of the form $R = kXY$ rather than $R = kX^2$, and thus the 2nd-order cross terms $^2R/ X Y$ are more important than the quadratic terms $^2R/ X^2$. In addition, the rate coefficient k is usually a function of temperature, adding another 2nd-order term $^2R/ X T$ (not evaluated here); and thus we can expect that correlated errors between temperature and a critical species will also cause notable error in the budgets.

4. Probability densities of critical species

The sensitivity analysis here helps us identify the critical species where a bias in the modeled distribution will produce a large bias in the budgets of O_3 and CH_4. The main species singled out here (NOx, O_3, CO, CH_4) are well known and CCMs often use these as standard measurement metrics. A surprise was the emergence of CH_3OOH as being important for P-O3, and a global climatology of this species should be a priority measurement. Although we have long known that H_2O and T are important factors (e.g., Table 2 of Holmes et al., 2013), these quantities have often been relegated to the physical climate system and not often though of a major source of model error in chemical system. Thus, when we are diagnosing the future tropospheric O_3 or CH_4 from the multi-model comparisons (Stevenson et al., 2013; Voulgarakis et al., 2013; Young et al., 2013, 2018; Griffiths et al., 2021), we need to document biases in T and H_2O.

Comparing T with mean profiles is straightforward, but H_2O is more difficult, even with profiles, because of the 3 orders of magnitude change over the troposphere. Thus, we recommend that relative humidity over liquid water (RHw, %) be used to detect bias. We show histograms of probability densities (PDs) of RHw from ATom-1234 in Figure 1c**.** We select the three tropical basin (C. Pacific, E. Pacific, Atlantic) and lower troposphere (0-6 km) because this is where most of the reactivity occurs (see Figure 1b). The ATom data for RHw show a clear bimodal distribution with extensive tropic regions having narrow PD with RHw $< 10\%$ and the bulk showing a broad PD about 80%. The E. Pacific has high seasonality with ATom-14 (the more reactive periods) lacking air with RHw $< 20\%$, consistent with the high reactivities noted above. PDs and for O_3, NOx and CO, as well as the 0-12 km PD for RHw, are shown in

Figures S34-S37. These gases show a wide range of seasonality, especially in the Pacific and provide a challenge for the models.

5. Conclusions

In terms of reactivities, by extending the ATom-1 (G2021) to the four seasons of ATom-1234, we find:

- The tropics dominate production of O_3, over at least the Pacific and Atlantic Ocean basins, with average P-O3 greater than 2 ppb/day throughout 0-12 km. Loss of O_3 and CH_4 are also tropical, but primarily at lower altitudes (0-6 km), and show similar seasonal shifts as P-O3, following the overhead sun. The northern mid-latitudes add a hot reactive season in the summer that is comparable to the tropics, but high reactivities are limited to below 8 km. There is no corresponding hot season for the southern mid-latitudes.
- Elevated levels of O_3 in the tropical Atlantic O_3 are known to be influenced by continental outflow of biomass burning from primarily Africa and also South America (Fishman et al., 1990), and here we find that the outflow is still actively producing O_3. High levels of L-O3 occur in a more tightly constrained region than P-O3, both in latitude and altitude (0-6 km), indicating a different process.
- The Eastern Pacific stands out: there are large, coherent reactive regions (20° in latitude by 2-3 km thick) associated with well mixed convective outflow from North America having extreme reactivities in both August (monsoonal) and May (biomass burning).
- The Arctic and Antarctic have much lower overall reactivity; and, given their small area, they play little role in the global O_3 and CH_4 budgets.

Our sensitivity analyses using ATom measurements has identified some clear direction and pitfalls, as well as providing a more robust view of chemical feedbacks:

- The critical species ($S > 0.1$) are NOx, O_3, CH_4, CO, and H_2O.
- While the sensitivities are linear for 0-20% perturbations, there are large 2^{nd}-order effects for coupled perturbations, comparable to 1^{st}-order sensitivities. Thus, coupled perturbations cannot be calculated simply from the sum of the linear sensitivities.
- Our 24-hour CH_4 feedback factor derived from ATom flights is similar to the global, steady-state feedback factors derived from global models over the past two decades.
- Our analysis presents quite a different picture of the lifetime of O_3 than is often assumed: if O_3 increases by 10%, then L-O3 increases by only 2.5% but P-O3 decreases by 5.4% and thus net loss increases by 7.9%. This

lengthens the effective timescale of a O_3 perturbation, especially since the regions of high P-O3 and L-O3 do not often coincide.

Probability densities for these critical species from ATom are presented as possible performance metrics for CCMs.

- Comparing H_2O with mean profiles is difficult because of the 3 orders of magnitude change over the troposphere, and thus, we recommend that relative humidity over liquid water (RHw) be used to detect model bias. Here we present a clear bimodal distribution of RHw in the tropics as measured by ATom.

The full ATom data set, including reactive species and the derived reactivities along with other atmospheric components describing the origins and processing of the air masses, provides the most extensive sampling of tropospheric chemistry over the remote ocean basins to date. The objective flight planning and near-continuous climb/descent profiling provided full sampling of the 0-12 km troposphere over the oceans. The statistics, including the co-variations of critical species (2D probability densities, in G2021), provide an excellent measurement metric for CCMs. The model-derived reactivities provide a testbed for the chemistry modules used in CCMs and also for independent analyses of the origins and chemical evolution of the air that matters, those chemically hot air masses clearly seen in the ATom flights. The sensitivity analysis of the 24-hour reactivities provides some core data that we feel should become a standard part of CCM evaluations and inter-comparisons. With this analysis, based on 10 s (2 km) air parcels, we believe we have partially deconstructed the spatial scales and variability that defines tropospheric chemistry.

Acknowledgements. The authors are indebted to the entire ATom Science Team including the managers, pilots and crew, who made this mission possible. We thank the instrument teams (co-authors on the first paper, Guo et al., 2021) for this valuable data set. Primary funding of the preparation of this paper at UC Irvine was through NASA grants NNX15AG57A and 80NSSC21K1454.

Data Availability. The full ATom data set as well as the derived MDS-2 and RDS*-2 data for ATom 1, 2, 3 and 4 are posted on the NASA ESPO ATom website (https://espo.nasa.gov/atom/content/ATom). The final archive for ATom data will be at Oak Ridge National Laboratory (ORNL), see https://daac.ornl.gov/ATOM/guides/ATom_merge.html. The MATLAB codes and data sets used in the analysis here are posted on Dryad (https://doi.org/10.7280/D1Q699), which has been expanded from Guo et al., 2021 to include this paper's data and codes.

References

Abalos, M., Orbe, C., Kinnison, D. E., Plummer, D., Oman, L. D., Jockel, P., Morgenstern, O., Garcia, R. R., Zeng, G., Stone, K. A., and Dameris, M. (2020) Future trends in stratosphere-to-troposphere transport in CCMI models, Atmos Chem Phys, 20(11), 6883-6901, 10.5194/acp-20-6883-2020.

Anderson, D. C., B. N. Duncan, A. M. Fiore, C. B. Baublitz, M. B. Follette-Cook, J. M. Nicely, and G. M. Wolfe (2021), Spatial and temporal variability in the hydroxyl (OH) radical: understanding the role of large-scale climate features and their influence on OH through its dynamical and photochemical drivers, Atmos Chem Phys, 21(8), 6481-6508, 10.5194/acp-21-6481-2021.

Brock, C. A., Froyd, K. D., Dollner, M., Williamson, C. J., Schill, G., Murphy, D. M., Wagner, N. J., Kupc, A., Jimenez, J. L., Campuzano-Jost, P., Nault, B. A., Schroder, J. C., Day, D. A., Price, D. J., Weinzierl, B., Schwarz, J. P., Katich, J. M., Wang, S. Y., Zeng, L. H., Weber, R., Dibb, J., Scheuer, E., Diskin, G. S., DiGangi, J. P., Bui, T., Dean-Day, J. M., Thompson, C. R., Peischl, J., Ryerson, T. B., Bourgeois, I., Daube, B. C., Commane, R., and Wofsy, S. C. (2021) Ambient aerosol properties in the remote atmosphere from global-scale in situ measurements, Atmos Chem Phys, 21(19), 15023-15063, 10.5194/acp-21-15023-2021.

Brune, W. H., Miller, D. O., Thames, A. B., Allen, H. M., Apel, E. C., Blake, D. R., Bui, T. P., Commane, R., Crounse, J. D., Daube, B. C., Diskin, G. S., DiGangi, J. P., Elkins, J. W., Hall, S. R., Hanisco, T. F., Hannun, R. A., Hintsa, E. J., Hornbrook, R. S., Kim, M. J., McKain, K., Moore, F. L., Neuman, J. A., Nicely, J. M., Peischl, J., Ryerson, T. B., St Clair, J. M., Sweeney, C., Teng, A. P., Thompson, C., Ullmann, K., Veres, P. R., Wennberg, P. O., and Wolfe, G. M. (2020): Exploring Oxidation in the Remote Free Troposphere: Insights From Atmospheric Tomography (ATom), J Geophys Res-Atmos, 125, ARTN e2019JD031685, 10.1029/2019JD031685.

Fishman, J., Watson, C. E., Larsen, J. C., and Logan, J. A. (1990), Distribution of Tropospheric Ozone Determined from Satellite Data, J Geophys Res-Atmos, 95, 3599-3617, 10.1029/Jd095id04p03599.

Griffiths, P. T., Murray, L. T., Zeng, G., Shin, Y. M., Abraham, N. L., Archibald, A. T., Deushi, M., Emmons, L. K., Galbally, I. E., Hassler, B., Horowitz, L. W., Keeble, J., Liu, J., Moeini, O., Naik, V., O'Connor, F. M., Oshima, N., Tarasick, D., Tilmes, S., Turnock, S. T., Wild, O., Young, P. J., and Zanis, P. (2021) Tropospheric ozone in CMIP6 simulations, Atmos Chem Phys, 21, 4187-4218, 10.5194/acp-21-4187-2021.

Guo, H., Flynn, C. M., Prather, M. J., Strode, S. A., Steenrod, S. D., Emmons, L., Lacey, F., Lamarque, J.-F., Fiore, A. M., Correa, G., Murray, L. T., Wolfe, G. M., St. Clair, J. M., Kim, M., Crounse, J., Diskin, G., DiGangi, J., Daube, B. C., Commane, R., McKain, K., Peischl, J., Ryerson, T. B., Thompson, C., Hanisco, T. F., Blake, D., Blake, N. J., Apel, E. C., Hornbrook, R. S., Elkins, J. W., Hintsa, E. J., Moore, F. L., and Wofsy, S., (2021). Heterogeneity and Chemical Reactivity of the Remote Troposphere defined by Aircraft Measurements, Atmos. Chem. Phys., 21, 13729–13746, 10.5194/acp-21-13729-2021.

Holmes, C. D. (2018). Methane feedback on atmospheric chemistry: Methods, models, and mechanisms. Journal of Advances in Modeling EarthSystems,10, 1087–1099. doi: 10.1002/2017MS001196.

Holmes, C. D., M. J. Prather, O. A. Sovde, and G. Myhre (2013), Future methane, hydroxyl, and their uncertainties: key climate and emission parameters for future predictions, Atmos Chem Phys, 13(1), 285-302, 10.5194/acp-13-285-2013.

Prather, M. J. (2009), Tropospheric O_3 from photolysis of O_2, Geophys. Res. Lett., 36, L03811, 10.1029/2008GL036851.

Prather, M.J., Flynn, C.M., Zhu, X., Steenrod, S.D., Strode, S.A., Fiore, A.M., Correa, G., Murray, L.T. and Lamarque, J.F., (2018). How well can global chemistry models calculate the reactivity of short-lived greenhouse gases in the remote troposphere, knowing the chemical composition. Atmospheric Measurement Techniques, 11(5), 2653-2668, https://doi.org/10.5194/amt-11-2653-2018.

Prather, M.J., Zhu, X., Flynn, C.M., Strode, S.A., Rodriguez, J.M., Steenrod, S.D., Liu, J., Lamarque, J.F., Fiore, A.M., Horowitz, L.W. and Mao, J., (2017). Global atmospheric chemistry–which air matters. Atmospheric Chemistry and Physics, 17(14), 9081-9102, 10.5194/acp-17-9081-2017.

Roelofs, G. J., and J. Lelieveld (1997), Model study of the influence of cross-tropopause O-3 transports on tropospheric O-3 levels, Tellus B, 49(1), 38-55, 10.1034/j.1600-0889.49.issue1.3.x.

Schill, G. P., Froyd, K. D., Bian, H., Kupc, A., Williamson, C., Brock, C. A., Ray, E., Hornbrook, R. S., Hills, A. J., Apel, E. C., Chin, M., Colarco, P. R., and Murphy, D. M. (2020), Widespread biomass burning smoke throughout the remote troposphere, Nat Geosci, 13, 422-425, 10.1038/s41561-020-0586-1, 2020.

Stevenson, D. S., Young, P. J., Naik, V., Lamarque, J. F., Shindell, D. T., Voulgarakis, A., Skeie, R. B., Dalsoren, S. B., Myhre, G., Berntsen, T. K., Folberth, G. A., Rumbold, S. T., Collins, W. J., MacKenzie, I. A., Doherty, R. M., Zeng, G., van Noije, T. P. C., Strunk, A., Bergmann, D., Cameron-Smith, P., Plummer, D. A., Strode, S. A., Horowitz, L., Lee, Y. H., Szopa, S., Sudo, K., Nagashima, T., Josse, B., Cionni, I., Righi, M., Eyring, V., Conley, A., Bowman, K. W., Wild, O., and Archibald, A., (2013), Tropospheric ozone changes, radiative forcing and attribution to emissions in the Atmospheric Chemistry and Climate Model Intercomparison Project (ACCMIP), Atmos Chem Phys, 13, 3063-3085, 10.5194/acp-13-3063-2013.

Strode, S. A., J. H. Liu, L. Lait, R. Commane, B. Daube, S. Wofsy, A. Conaty, P. Newman, and M. Prather (2018), Forecasting carbon monoxide on a global scale for the ATom-1 aircraft mission: insights from airborne and satellite observations and modeling, Atmos Chem Phys, 18(15), 10955-10971, 10.5194/acp-18-10955-2018.

Thompson, C. R., Wofsy, S. C., Prather, M. J., Newman, P. A., Hanisco, T. F., Ryerson, T. B., Fahey, D. W., Apel, E. C., Brock, C. A., Brune, W. H., Froyd, K., Katich, J. M., Nicely, J. M., Peischl, J., Ray, E., Veres, P. R., Wang, S., Allen, H. M., Asher, E., Bian, H., Blake, D., Bourgeois, I., Budney, J., Bui, T. P., Butler, A., Campuzano-Jost, P., Chang, C., Chin, M., Commane, R., Correa,

G., Crounse, J. D., Daube, B., Dibb, J. E., Digangi, J. P., Diskin, G. S., Dollner, M., Elkins, J. W., Fiore, A. M., Flynn, C. M., Guo, H., Hall, S. R., Hannun, R. A., Hills, A., Hintsa, E. J., Hodzic, A., Hornbrook, R. S., Huey, L. G., Jimenez, J. L., Keeling, R. F., Kim, M. J., Kupc, A., Lacey, F., Lait, L. R., Lamarque, J., Liu, J., Mckain, K., Meinardi, S., Miller, D. O., Montzka, S. A., Moore, F. L., Morgan, E. J., Murphy, D. M., Murray, L. T., Nault, B. A., Neuman, J. A., Nguyen, L., Gonzalez, Y., Rollins, A., Rosenlof, K., Sargent, M., Schill, G., Schwarz, J. P., St. Clair, J. M., Steenrod, S. D., Stephens, B. B., Strahan, S. E., Strode, S. A., Sweeney, C., Thames, A. B., Ullmann, K., Wagner, N., Weber, R., Weinzierl, B., Wennberg, P. O., Williamson, C. J., Wolfe, G. M., & Zeng, L., (2021), The NASA Atmospheric Tomography (ATom) Mission: Imaging the Chemistry of the Global Atmosphere, Bulletin of the American Meteorological Society, on-line release, 10.1175/bams-d-20-0315.1.

Travis, K. R., Heald, C. L., Allen, H. M., Apel, E. C., Arnold, S. R., Blake, D. R., Brune, W. H., Chen, X., Commane, R., Crounse, J. D., Daube, B. C., Diskin, G. S., Elkins, J. W., Evans, M. J., Hall, S. R., Hintsa, E. J., Hornbrook, R. S., Kasibhatla, P. S., Kim, M. J., Luo, G., McKain, K., Millet, D. B., Moore, F. L., Peischl, J., Ryerson, T. B., Sherwen, T., Thames, A. B., Ullmann, K., Wang, X., Wennberg, P. O., Wolfe, G. M., and Yu, F. Q. (2020), Constraining remote oxidation capacity with ATom observations, Atmos Chem Phys, 20, 7753-7781, 10.5194/acp-20-7753-2020.

Veres, P. R., Neuman, J. A., Bertram, T. H., Assaf, E., Wolfe, G. M., Williamson, C. J., Weinzierl, B., Tilmes, S., Thompson, C. R., Thames, A. B., Schroder, J. C., Saiz-Lopez, A., Rollins, A. W., Roberts, J. M., Price, D., Peischl, J., Nault, B. A., Moller, K. H., Miller, D. O., Meinardi, S., Li, Q. Y., Lamarque, J. F., Kupc, A., Kjaergaard, H. G., Kinnison, D., Jimenez, J. L., Jernigan, C. M., Hornbrook, R. S., Hills, A., Dollner, M., Day, D. A., Cuevas, C. A., Campuzano-Jost, P., Burkholder, J., Bui, T. P., Brune, W. H., Brown, S. S., Brock, C. A., Bourgeois, I., Blake, D. R., Apel, E. C., and Ryerson, T. B. (2020), Global airborne sampling reveals a previously unobserved dimethyl sulfide oxidation mechanism in the marine atmosphere, P Natl Acad Sci USA, 117, 4505-4510, 10.1073/pnas.1919344117.

Voulgarakis, A., Naik, V., Lamarque, J. F., Shindell, D. T., Young, P. J., Prather, M. J., Wild, O., Field, R. D., Bergmann, D., Cameron-Smith, P., Cionni, I., Collins, W. J., Dalsoren, S. B., Doherty, R. M., Eyring, V., Faluvegi, G., Folberth, G. A., Horowitz, L. W., Josse, B., MacKenzie, I. A., Nagashima, T., Plummer, D. A., Righi, M., Rumbold, S. T., Stevenson, D. S., Strode, S. A., Sudo, K., Szopa, S., and Zeng, G., (2013), Analysis of present day and future OH and methane lifetime in the ACCMIP simulations, Atmos Chem Phys, 13, 2563-2587, 10.5194/acp-13-2563-2013.

Williamson, C. J., Kupc, A., Rollins, A., Kazil, J., Froyd, K. D., Ray, E. A., Murphy, D. M., Schill, G. P., Peischl, J., Thompson, C., Bourgeois, I., Thomas, B. R. A., Diskin, G. S., DiGangi, J. P., Blake, D. R., Bui, T. P. V., Dollner, M., Weinzierl, B., and Brock, C. A. (2021), Large hemispheric difference in

nucleation mode aerosol concentrations in the lowermost stratosphere at mid- and high latitudes, Atmos Chem Phys, 21, 9065-9088, 10.5194/acp-21-9065-2021.

Wofsy, S.C., et al. (2018), ATom: Merged Atmospheric Chemistry, Trace Gases, and Aerosols. ORNL DAAC, Oak Ridge, Tennessee, USA. 10.3334/ORNL-DAAC/1581.

Wolfe, G. M., Nicely, J. M., Clair, J. M. S., Hanisco, T. F., Liao, J., Oman, L. D., Brune, W. B., Miller, D., Thames, A., Abad, G. G., Ryerson, T. B., Thompson, C. R., Peischl, J., McCain, K., Sweeney, C., Wennberg, P. O., Kim, M., Crounse, J. D., Hall, S. R., Ullmann, K., Diskin, G., Bui, P., Chang, C., and Dean-Day, J. (2019), Mapping hydroxyl variability throughout the global remote troposphere via synthesis of airborne and satellite formaldehyde observations, P Natl Acad Sci USA, 116, 11171-11180, 10.1073/pnas.1821661116.

Young, P. J., Naik, V., Fiore, A. M., Gaudel, A., Guo, J., Lin, M. Y., Neu, J. L., Parrish, D. D., Rieder, H. E., Schnell, J. L., Tilmes, S., Wild, O., Zhang, L., Ziemke, J., Brandt, J., Delcloo, A., Doherty, R. M., Geels, C., Hegglin, M. I., Hu, L., Im, U., Kumar, R., Luhar, A., Murray, L., Plummer, D., Rodriguez, J., Saiz-Lopez, A., Schultz, M. G., Woodhouse, M. T., and Zeng, G., (2018) Tropospheric Ozone Assessment Report: Assessment of global-scale model performance for global and regional ozone distributions, variability, and trends, Elementa-Science of the Anthropocene, 6, 10.1525/elementa.265.

Table 1. First-order sensitivities of the reactivities (R) with respect to the dominant species (X), S [ln(R)]/ [ln(X)] (%/%) are calculated with a perturbation of 10%. Results are averaged over ATom-1234 for Pacific and Atlantic basins (54°S to 60°N), and the standard deviation is shown. The H_2O results include only ATom-1. The CTM results are calculated using the chemical species from the UCI CTM on 16 August 2016 as the initial conditions, and separate large Pacific and Atlantic blocks are used (see Figure S1 of G2021) and airmass weighted, with the average of the 2 basins shown here. For the expanded ATom table showing Pacific and Atlantic, and the 4 deployments separately, plus the other species (HCHO, H_2O_2, PAN, HNO_3, HNO_4, CH_3OOH, C_2H_6, C_{3+}-alkanes) see Supplemental Table S1.

X	**P-O3**	**L-O3**	**L-CH4**						
	ATom	*s.d.*	*CTM*	*ATom*	*s.d.*	*CTM*	*ATom*	*s.d.*	*CTM*
NOx	**0.21**	*0.02*	**0.19**	0.04	*0.01*	0.03	**0.09**	*0.01*	**0.11**
O_3	**-0.54**	*0.04*	**-0.53**	**0.25**	*0.03*	**0.23**	**0.36**	*0.03*	**0.40**
CH_4	**0.15**	*0.01*	**0.16**	-0.02	*0.01*	-0.02	**0.71**	*0.02*	**0.69**
CO	0.07	*0.01*	0.07	0.00	*0.00*	0.00	**-0.38**	*0.02*	**-0.35**
H_2O	**0.14**	*0.00*	**0.14**	**0.48**	*0.01*	**0.47**	**0.38**	*0.01*	**0.37**

Table 2. Second-order, cross-term sensitivities of the reactivity L-CH4 relative

to critical species (NOx, O_3, CH_4, CO) calculated in pair combinations. Results here are from ATom-1 and the Pacific basin (54°S-60°N). The single +10% sensitivities calculated for individual species, S(X+10%), are shown in italics along the diagonal. The doubly signed (i.e., ++ or --) off-diagonal values represent the additional change in sensitivity due to the coupling of the two species: S(X+10% & Y+10%) – S(X+10%) – S(Y+10%). When the 2nd-order is small (only the O_3 x CO term here), the coupled perturbation is simply the sum of the two individual ones. Atom-1 results for other reactivities (P-O3, L-O3) and the Atlantic basin are given in Supplemental Table S3.

	Pacific			
L-CH4	NOx	O_3	CH_4	CO
NOx	*+0.09*	**--0.13**	**--0.18**	**++0.12**
O_3		*+0.39*	**--0.19**	**--0.01**
CH_4			*+0.69*	**--0.12**
CO				*-0.34*

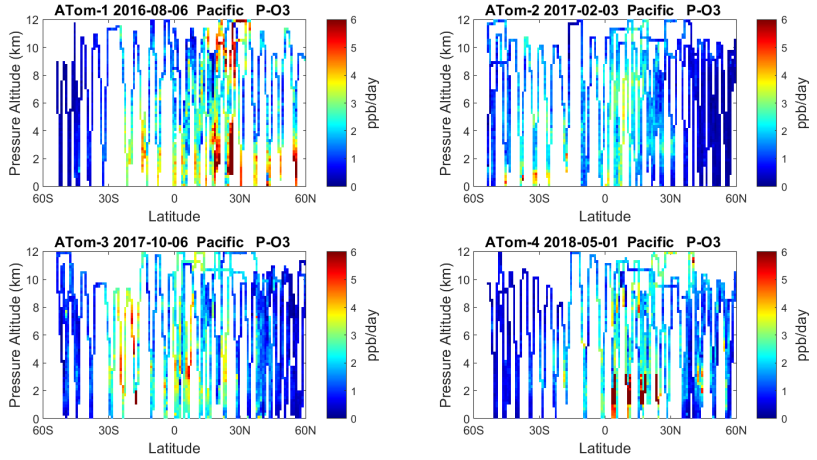

(a)

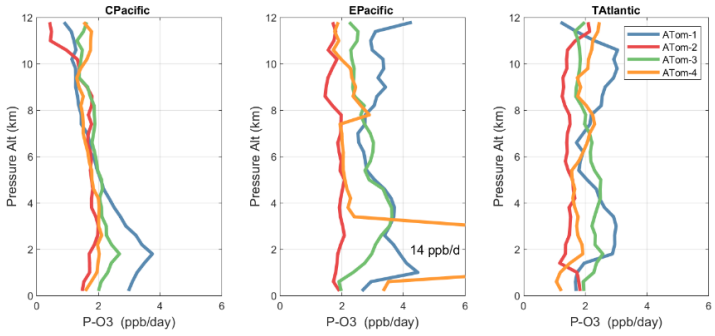

(b)

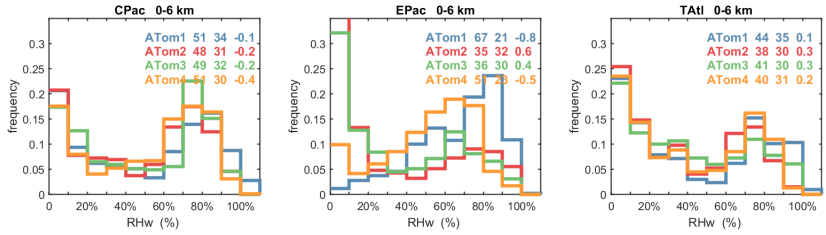

(c)

Figure 1. **(a)** Curtain plots for P-O3 (0-6 ppb/d) showing the profiling of the 4 ATom deployments over the